Geophys. J. Int. (1993) **114,** 635–650

A Simple Model of Plate Generation from Mantle Flow

David Bercovici*

Department of Geology & Geophysics
School of Ocean & Earth Science & Technology
University of Hawaii, Honolulu
* Now at Department of Geology & Geophysics, Yale University

SUMMARY

A simple model of non-Newtonian creeping flow is used to evaluate classes of rheologies which allow viscous mantle flow to become plate-like. The model describes shallow-layer lithospheric motion driven by sources and sinks. The sources represent spreading ridges while the sinks represent subduction zones; the sources and sinks thus also prescribe the poloidal component of the surface flow field. The toroidal (strike-slip) component of the flow field is found via the solution of the Stokes equation with non-Newtonian rheology. As a first basic investigation of the model, the horizontal divergence from the two-dimensional rectangular velocity field of Olson & Bercovici (1991) is used for the source-sink field. The degree to which the induced fluid flow reproduces the rectangular plate is used to measure the success of different rheologies in generating plate-like flows. Results indicate that power-law rheologies, even in the limit of very high power-law index ν, can only produce modest plate-like flow. For example, the ratio of toroidal to poloidal kinetic energy for a source-sink field derived from a square plate is at best 0.65, whereas a perfect square plate has a ratio of 1.0. Moreover, the power-law rheology appears to reach an asymptotic limit in its ability to produce plate-like behavior. This implies that plate tectonics is unlikely to arise from a power-law rheology even in the limit of very high ν. A class of rheologies that yield significantly more promising results arise from the Carreau pseudo-plastic rheology with the power-law index taken to be $\nu < 0$. One rheology in this class is the continuum model for stick-slip, earthquake behavior of Whitehead & Gans (1974), which is essentially the Carreau equation with $\nu = -1$. This class of rheologies, referred to as the stick-slip rheologies, induces a toroidal to poloidal kinetic energy ratio for a square plates's source-sink function which can be as high as 0.9. The viscosity (or strength) distribution for this class of rheologies also appears more plate-like, showing fairly uniform high viscosity regions (pseudo-plates) and sharply defined low viscosity zones (pseudo-margins). In contrast, even the most nonlinear power-law rheology produces spatially varying high viscosity regions and relatively smooth low viscosity margins. The greater success of the stick-slip rheologies in producing plates is attributed to a self-lubricating mechanism in which the transfer of momentum from regions of high shear to low shear is inhibited. In contrast, even in the limit of infinite power-law index, a power-law rheology can retard but never prohibit momentum transfer. This feature is essential to the sharpening of velocity profiles into plate-like profiles, which is illustrated with a simple boundary-layer theory.

Key words: Plate tectonics, mantle convection, non-Newtonian flow, toroidal-poloidal coupling.

1 INTRODUCTION

One of the major quandaries in geodynamics concerns the relation between plate tectonics and mantle convection. The proposition that mantle convection is the driving force of surface motion is nearly as old as the original theory of continental drift (e.g., Holmes 1928). In the years since the modern theory of plate tectonics arose, much has been done to explain not only the nature of mantle convection but how it may drive the plates. A majority of work has been concerned with the interaction between existing plates and mantle flow. This area of research has lead to a large number of significant results, from the prediction of subduction dip angle with plate driven mantle flow (Hager & O'Connell 1978,1979), to the determination of vertical viscosity structure from flows driven by mantle density heterogeneity and plate forces (Hager & O'Connell 1981; Forte & Peltier 1987; Ricard, Froidevaux & Fleitout 1988; Ricard & Vigny 1989; Ricard & Bai 1991; Forte, Peltier & Dziewonski 1991). Fully dynamic models of nonlinear thermal convection with surface plates have also been developed to investigate the feedback between plate motion and the underlying mantle flow (Olson & Corcos 1980; Davies 1986, 1989; Gurnis 1988; Cserepes & Christensen, 1990; Gable, O'Connell & Travis 1991; King, Gable & Weinstein 1992). These studies have provided considerable insight into topics ranging from the mechanisms of continental breakup and formation (Gurnis 1988) to the interaction of strike-slip motion and mantle convection (Gable et al. 1991).

In many of the above studies the plates are assumed to be preexisting rafts floating on the mantle. However, mantle convection and plate tectonics are more than simply mechanically coupled. The plates are, in fact, an integral part of the mantle circulation: they are clearly formed at ridges and recirculate into the mantle through subduction zones. In essence, plate tectonics is the surface expression of mantle convection. The most fundamental, and perhaps most difficult goal in the unification of plate tectonics and mantle dynamics is understanding the mechanics by which plate tectonics arises from a convecting mantle.

There are several aspects of the plate-tectonic style of mantle convection that are characteristic of simple fluid dynamic models of thermal convection. The oceanic lithosphere is fairly well described as a thermal boundary layer of mantle convection (Turcotte & Oxburgh 1967). Subducting slabs and hotspot-inferred mantle plumes are also strongly suggestive of sheet-like downwellings and columnar upwellings obtained in many forms of three-dimensional convection (Houseman 1988; Bercovici, Schubert & Glatzmaier 1989). That mid-ocean ridges are likely not the result of active upwelling (Lachenbruch 1976) correlates with the fact that sheet-like upwellings are fairly rare in convecting systems (Bercovici et al. 1989).

However, there are also many aspects of plate tectonics that are not characteristic of simple thermal convection. Subducting slabs represent asymmetric downwelling – i.e., only one plate at the convergent zone actually sinks – which is not obtainable with a simple model of mantle convection (Gurnis & Hager 1988; King & Hager 1990). Passive rifting also cannot occur in basic fluid models of mantle flow. However, the most conspicuous feature missing from basic convection models is strike-slip motion along transform faults and oblique subduction zones; this motion is also called toroidal flow. While the net kinetic energy of strike-slip motion is nearly comparable to the net kinetic energy of plate motions at convergent/divergent boundaries (called poloidal flow) (Hager & O'Connell 1978), no strike-slip motion of any kind can be predicted by simple convection theory (i.e., with constant or depth dependent viscosity). Lateral variations in viscosity, either throughout the whole mantle or at the very least in the lithosphere itself are required to allow strike-slip motion.

Most features of plate tectonics not accounted for in simple models of convection are generally attributed to the various complicated deformation mechanisms in the mantle and/or lithosphere (Hager & O'Connell 1978, 1979; Kaula 1980). Thus, a working hypothesis for investigating the relation between the plates and mantle is that the plates – their geometry and motions – arise from the interaction of the Earth's complicated rheology and the mantle flow itself. To understand how plate-tectonics is generated from mantle convection, it is important to consider the entire plate-mantle system as a single medium with a complex rheology.

The complex rheology necessary to produce the plate-tectonic style of mantle convection is, however, not immediately obvious. It is generally assumed that plate-like behavior is due primarily to the interaction of convective flow with a plastic or pseudo-plastic rheology (wherein the viscosity is stress dependent such that the fluid weakens with an increase in stress). Numerical models of convection in non-Newtonian fluid have shown a variety of results, from the verdict that non-Newtonian rheology has little effect on two-dimensional flows (Parmentier, Turcotte & Torrance 1976; Parmentier 1978; Parmentier & Morgan 1982) to quite significant effects when coupled to temperature-dependence of viscosity (Cserepes 1982; Christensen 1984). Weinstein & Olson (1992) showed that for two-dimensional convection beneath a non-Newtonian fluid lithosphere, a power-law rheology with index up to 7 is required to create strong plate-like interiors and weak plate margins. However, one of the most important effects of non-Newtonian rheology can only happen in three dimensions; i.e., the generation of toroidal or strike-slip motion. Christensen & Harder (1991), presenting the only three-dimensional numerical model of non-Newtonian convection to date, showed how even when the power-law index is taken up to 6 (whereas mantle rheology is characterized by an index of 3), the toroidal motion accounts for only 10% of the net kinetic energy. In the Earth's plate motions, toroidal energy comprises closer to 44% (Hager & O'Connell 1978; Forte & Peltier 1987). The coupling mechanics between poloidal and toroidal flow for spherical geometry was investigated analytically by Ribe (1992) to show how the spherical harmonic modes in toroidal energy respond through certain selection rules to a given buoyancy interacting with laterally varying lithospheric stiffness (a combination of lithospheric viscosity and thickness). A further clue regarding the physics of toroidal-poloidal coupling was provided by O'Connell, Gable & Hager (1991) who demonstrated with Monte Carlo methods that the present day plate motions minimize the toroidal kinetic energy. However, the physical mechanism by which the interaction of flow and rheology creates distinct plates with strike-slip margins is not well understood. Olson & Bercovici (1991), using simple statistical arguments, hypothesized that the present state of toroidal-poloidal near equipartitioning occurs because plastic or pseudo-plastic rheology causes the plates (and the underlying convection cell, if one is present) to be decoupled from each other to the extent that the plates drift nearly independently of one another.

One of the primary limitations in the studies of how plate-like flows are generated from non-Newtonian thermal convection is that they involve strongly nonlinear models of convection itself which are numerically intensive, especially in the three-dimensions necessary to obtain toroidal motion (Christensen & Harder 1991). A further limitation on these models is the use of mantle-like power-law rheologies. Such rheologies are empirically determined in isothermal viscometric flows (uni-directional shear flow) or uniaxial extension/compression (Weertman & Weertman 1975; Ranalli 1987). These rheologies might possibly have little to do with the actual rheology of the plate-mantle system as a whole, with its distinct three-dimensional flow, occurrence of lithospheric failure mechanisms, extensive volatile entrainment, viscous heating, etc.

In this study we present a simple model of non-Newtonian flow that does not explicity involve convection. By its simplicity we alleviate some of the numerical restrictions encountered by rigorous models of convection. In this model, toroidal motion is restricted to the lithosphere which we assume is a shallow fluid layer (see also Ribe 1992; Weinstein & Olson 1992). Moreover, as the toroidal flow is, in the end, driven by poloidal flow (i.e., it has no energy source other than its mechanical coupling to poloidal motion), we assume all flow is driven by a prescribed poloidal velocity potential. In other words, the model involves two-dimensional flow driven by sources and sinks; the sources and sinks represent divergent and convergent zones (or upwellings and downwellings), respectively. The model is thus both kinematic (in that it prescribes the poloidal component of the flow field) and dynamic (in that it solves for the toroidal componenent of the flow field from the equations of motion). An important caveat is that since the poloidal flow is prescribed, the model can only partially examine the interaction of rheology and flow; it does not account for the rheological effects at divergent and convergent margins (e.g., rifting and subduction zone dynamics). The model can only allow us to examine how strike-slip motion arises from the interaction of a given poloidal field with a particular rheology.

The primary purpose of this study is to determine the best rheology with which a given poloidal flow field can excite significant toroidal motion. While we primarily concentrate on strain-rate softening rheologies, we do not limit ourselves to a mantle-like power-law viscosity. In this paper, we examine a simple Cartesian version of the model using idealized but well calibrated test cases to elucidate the more basic physics of plate generation. In a later companion paper, we apply this to the real Earth. The present day plate motions are an ideal data set for this model in that we can impose the observed horizontal divergence of the Earth's plates on a thin non-Newtonian spherical fluid shell (representing the Earth's lithosphere) and examine what rheologies lead to the best reproduction of the observed strike-slip motion, and hence generation of the actual tectonic plates themselves.

2 THEORY

2.1 Model Assumptions

We model the Earth's lithosphere – defined for our purposes as the upper boundary layer of mantle convection – as a shallow, constant thickness, incompressible layer of non-Newtonian fluid in Cartesian geometry, bounded above and below by relatively inviscid media, i.e., the atmosphere above and a low viscosity asthenosphere below. The relevance of this model to the Earth hinges to a large extent on the assumption of a relatively inviscid asthenosphere, thus this assumption deserves some discussion. The inviscid asthenosphere assumption is valid as long as the viscosity of the lithospheric layer is everywhere much greater than the asthenospheric viscosity. This assumption may be compromised in cases with highly non-Newtonian rheologies in which rapidly deforming regions may have very low viscosity. However, the viscosity contrast between the lithosphere and asthenosphere is conservatively between 10^5 and 10^7 (where the asthenospheric viscosity is between 10^{18} and 10^{20} $Pa\ s$ while a typical lithospheric viscosity is 10^{25} $Pa\ s$ or higher; see Beaumont, 1976; Watts, Karner & Steckler 1982). Therefore, an extremely large viscosity drop from plate interior to plate margin would be required to invalidate this model. Such an intraplate viscosity drop, however, can neither be excluded nor assumed, as it has never been quantified for the Earth. In this study, the model viscosity drop within the fluid layer is typically three orders of magnitude – much less than the Earth's lithosphere-asthenosphere viscosity contrast – and is thus at least self-consistent as a model of the lithosphere.

The inviscid asthenosphere approximation also implicitly assumes that all forces balance within the lithospheric layer, and thus basal tractions are negligible. Studies of forces on the tectonic plates have yielded varied conclusions about the influence of viscous drag from the asthenosphere. Forsyth & Uyeda (1975) found that the independence of plate velocity on plate area was indicative of negligible asthenospheric drag. However, in that study, ridge push was modelled as an edge force. Hager & O'Connell (1981) modelled ridge push as a force associated with lithospheric thickening distributed over the area of the plate. Neither this force nor asthenospheric drag are negligible, however they tend to cancel, thus also leading to plate velocities independent of plate area. The model presented in this study can more or less accommodate either conclusion regarding viscous drag. A negligible asthenospheric drag is explicitly in keeping with the inviscid asthenosphere approximation. On the other hand, as this model also does not account for lithospheric thickening, one may argue that distributed ridge push and asthenospheric drag balance and are thus cancelled out in the model. Naturally, this latter argument is problematic as it is never safe to assume that the mantle flow forcing or being forced by lithospheric motion is easily predictable. The model may be made more realistic by the inclusion of underlying viscous drag and layer thickening, though by the conclusions of Hager & O'Connell (1981) it is probably wiser to assume these effects cancel than to include one without the other. Nevertheless, these effects can eventually be incorporated into a shallow layer model such as the one presented here, as was shown by Ribe (1992) and Weinstein & Olson (1992). As this would introduce extra complications and degrees of freedom, we presently opt for a simpler model to examine the more basic physics of non-Newtonian lithospheric flow.

2.2 Equations of Motion

Given the above considerations, the boundaries of the layer are assumed to be free-slip surfaces. With these boundary conditions, and the narrowness of the layer, we further assume that there is no variation of stress or velocity with depth across the layer, and only horizontal velocities exist in the layer. To drive the flow, we prescribe mass sources and sinks, or, equivalently, the horizontal divergence, in the layer; thus upwelling appears as sources, downwelling as sinks. Our field of souces and sinks is described by the source-sink function $S(x,y)$ (where x and y are the two horizontal coordinates) wherein, by continuity,

$$\nabla_h \cdot \underline{v} = \frac{\partial u}{\partial x} + \frac{\partial v}{\partial y} = S \tag{1}$$

where $\nabla_h = (\frac{\partial}{\partial x}, \frac{\partial}{\partial y}, 0)$ is the horizontal gradient operator, and $\underline{v} = (u, v, w)$ is the Cartesian velocity vector. There is no vertical flow in the layer itself. However, because of the sources and sinks, there is implicitly a nonzero vertical gradient in the vertical velocity; i.e., by equation (1), $\frac{\partial w}{\partial z} = -S$.

We next define the horizontal velocity vector $\underline{v_h} = (u, v, 0)$ by a Helmholtz representation:

$$\underline{v_h} = \nabla_h \phi + \nabla_h \times (\psi \hat{z}) \tag{2}$$

where ϕ is a velocity potential representing the poloidal flow (in fact $\phi = \frac{\partial W}{\partial z}$ where $W\hat{z}$ is the poloidal velocity vector potential) and ψ is the horizontal stream function; $\psi\hat{z}$ is exactly equivalent to the toroidal velocity vector potential. Combining equations (1) and (2), we see that ϕ obeys Poissons equation:

$$\nabla_h^2 \phi = S \tag{3}$$

thus, specifying the sources and sinks through S directly prescribes the poloidal potential ϕ. All that remains is to determine ψ.

The stream function ψ is found through the Stokes equation for conservation of momentum

$$0 = -\nabla P + \nabla \cdot (2\eta \underline{\underline{\dot{e}}}) \tag{4}$$

where P is the nonhydrostatic pressure (such that body forces and hydrostatic pressure have been removed), $\underline{\underline{\dot{e}}} = \frac{1}{2}(\nabla \underline{v} + [\nabla \underline{v}]^\dagger)$ is the strain-rate tensor, and η is the non-Newtonian laterally varying viscosity which is a function of ϕ and ψ. For now, we simply define η as a general function of x and y until specifying a rheology later. To obtain an equation for ψ, we take $\hat{z}\cdot\nabla\times$ of equation (4); with the assumptions that u, v and thus η are independent of z (because of the free-slip boundaries and shallow layer), and that $w = \frac{\partial w}{\partial x} = \frac{\partial w}{\partial y} = 0$ while $\frac{\partial w}{\partial z} = -S$ in the layer, we arrive at

$$\eta\nabla_h^4\psi \quad + \quad 2\nabla_h\eta\cdot\nabla_h\nabla_h^2\psi + \Delta^*\eta\Delta^*\psi + 4\frac{\partial^2\eta}{\partial x\partial y}\frac{\partial^2\psi}{\partial x\partial y} = \hat{z}\cdot\nabla_h\eta\times\nabla_h S + 2\Delta^*\eta\frac{\partial^2\phi}{\partial x\partial y} - 2\frac{\partial^2\eta}{\partial x\partial y}\Delta^*\phi \quad (5)$$

where $\Delta^* = \frac{\partial^2}{\partial x^2} - \frac{\partial^2}{\partial y^2}$. Equation (5) is an inhomogeneous equation for ψ being forced by potential (or source-sink) flow via gradients in viscosity. If η is constant, equation (5) becomes a homogeneous biharmonic equation for ψ yielding a null solution (i.e., $\psi = 0$) if the boundary conditions are homogeneous (as they are bound to be unless an artificial source of toroidal motion is supplied at some boundary in the (x, y) domain).

Before explicitly defining a rheology, we simply assume that $\eta = \eta_o\tilde{\eta}(x, y)$ where $\tilde{\eta}$ is a dimensionless viscosity. We also define the domain of interest as $-L_x \le x \le L_x$, $-L_y \le y \le L_y$ and assume a density of the fluid layer ρ. Nondimensionalizing x and y by L_x (such that the domain now lies in the range $-1 \le x, y/b \le 1$ where $b = L_y/L_x$), η by η_o, ψ and ϕ by η_o/ρ, and S by $\eta_o/(\rho L_x^2)$, we simply regain equation (5), dropping the tilde on $\tilde{\eta}$. The dimensionless equation (5) is then solved by a spectral-transform, under-relaxation method (see Appendix and Christensen and Harder, 1991).

2.3 Rheology

The rheology we employ in this study accounts for nonlinear plastic-type behavior in which the fluid viscosity decreases with an increase in strain-rate (or stress); this rheology is most likely to yield plate-like flows as it is necessary for creating weak plate margins (regions of high deformation) and strong plate interiors (regions of little deformation).

As the source-sink flow described here is strictly isothermal, viscosity cannot be explicitly dependent on temperature. However, we can approximate temperature dependence by noting that in convective flows, temperature is usually strongly correlated with either vertical velocity (in the deep interior regions where horizontal velocities are small) or horizontal divergence (near the surface where vertical velocities are small); i.e., fluid is generally hot (cold) where it is either upwelling (downwelling) in the deep mantle or diverging (converging) at the Earth's surface. Thus, it is possible to approximate temperature by some linear combination of w and $\nabla_h\cdot\underline{v} = S$. This can then be employed in a temperature-dependent rheology. Although we will not investigate this effect here, we note it for future reference.

For generality, we employ the following equation for dimensionless viscosity

$$\eta = (\gamma + \dot{e}^2)^{(1/\nu-1)/2} \qquad (6a)$$

where

$$\dot{e}^2 = \underline{\underline{\dot{e}}} : \underline{\underline{\dot{e}}} = 2\left[\left(\frac{\partial u}{\partial x}\right)^2 + S^2 - S\frac{\partial u}{\partial x}\right] + \frac{1}{2}\left(\frac{\partial u}{\partial y} + \frac{\partial v}{\partial x}\right)^2 \qquad (6b)$$

is the second invariant of the strain-rate tensor (within a factor of

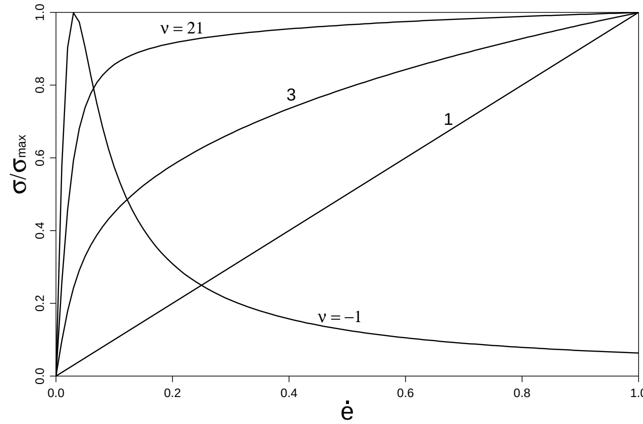

Figure 1. Stress versus strain-rate relation of equation (7) for the viscosity of equation (6) with various values of the power-law index ν. Power-law rheologies corresponding to values of $\nu \ge 1$ are shown, along with the Whitehead-Gans (W-G) stick-slip rheology with $\nu = -1$. For all curves $\gamma = 10^{-3}$. Stress is normalized by its maximum value σ_{max}; for the power-law cases $\sigma_{max} = 1$, while for the W-G case $\sigma_{max} = (2\sqrt{\gamma})^{-1}$.

-2). This equation is essentially a simplification of the Carreau rheology (see Bird, Armstrong & Hassager 1987) for pseudo-plastic flows. In the limit of $\gamma \to 0$, the basic power-law Ostwald-de Waele rheology is recovered. We retain the parameter γ to proscribe viscosity singularities (in the cases where $1/\nu - 1 < 0$ and $\dot{e}^2 = 0$) and hence prescribe a maximum value of η. The parameter ν is the power-law index for $\nu > 0$, where dilatancy (i.e., strain-rate hardening) occurs if $\nu < 1$ and pseudo-plasticity (strain-rate softening) if $\nu > 1$. The rheologies with $\nu > 1$ are typical of those used in geodynamical studies of non-Newtonian flow. Another special class of rheologies exists for $\nu < 0$. These rheologies are also strain-rate softening. However, they further allow stress to build up toward a maximum value with increasing strain-rate and then be released with increased deformation; i.e., they induce a stress cut-off (Figure 1). If we consider the root-mean-square stress scalar (i.e, the square-root of the second stress invariant)

$$\sigma = \sqrt{\underline{\underline{\sigma}} : \underline{\underline{\sigma}}} = 2\eta\dot{e} \qquad (7)$$

(where $\underline{\underline{\sigma}}$ is the deviatoric viscous stress tensor), then stress is maximized at $\dot{e} = \pm\sqrt{-\nu\gamma}$. A stress maximum can thus occur at a real value of $\dot{e}$ for $\nu < 0$. Beyond the stress maximum (i.e., for $|\dot{e}| > \sqrt{-\nu\gamma}$), the material is self-lubricating in that the faster it deforms the less it resists deformation. The occurence of a stress maximum has importance in this problem because, as will be shown later, it allows plate-like flows to sharpen their velocity profiles, rather than spread their profiles by the outward transfer of momentum. This class of rheologies is also important as a continuum model of stick-slip behavior. That is, it can model the rapid build up of stress with little strain-rate, followed by the release of stress once the cut-off strain-rate (i.e., the $\dot{e}$ at which the stress maximum occurs) is exceeded. Such a rheology was used for the case of $\nu = -1$ by Whitehead & Gans (1974) in their simple yet elegant zero-dimensional continuum model of earth-quake behavior; this rheology leads to a nonlinear harmonic oscillator that yields a nearly saw-tooth periodicity highly suggestive of stress build-up and release during earth-quake sequences. Similar constitutive relations have also been used in kinematic dynamo theory to relate the "α" parameter to magnetic induction $\underline{B}$; this is termed "quenching" in the dynamo literature and leads to a nonlinear B-field oscillator suggestive of geomagnetic field reversals (e.g., Olson & Hagee 1990; see Roberts & Soward 1991).

The class of rheologies for $\nu < 0$ will be referred to as stick-slip rheologies. They are in fact merely theoretical rheologies that have no empirical basis. However, as Whitehead & Gans (1974) demonstrated, the rheology with $\nu = -1$ can arise, in a simplified sense, from the combination of temperature-dependent viscosity and shear heating. This combination was also shown to yield an inverse dependence of stress on plate velocity and thus a self-lubricating mechanism for shallow mantle flow (Schubert & Turcotte 1972), as well as surge behavior in glaciers (Yuen & Schubert 1979). If we assume a simplified temperature-dependent viscosity (Whitehead & Gans 1974)

$$\eta = \eta_o[1 - \alpha'(T - T_o)] \tag{8}$$

and a steady-state relation between shear heating and thermal diffusion

$$K(T - T_o) = \eta \dot{e}^2 \tag{9}$$

(where K is a heat transfer coefficient) then elimination of the temperature anomaly $T - T_o$ between equations (8) and (9) yields

$$\eta = \frac{K/\alpha'}{K/(\alpha'\eta_o) + \dot{e}^2} \tag{10}$$

Thus, in an idealized way, rheologies with $\nu < 0$ potentially account for nonisothermal behavior at zones of high deformation. As the rheology for $\nu = -1$ is most physically justifiable, we will concentrate to some extent on that case; this rheology will be refered to as the Whitehead-Gans, or W-G, stick-slip rheology.

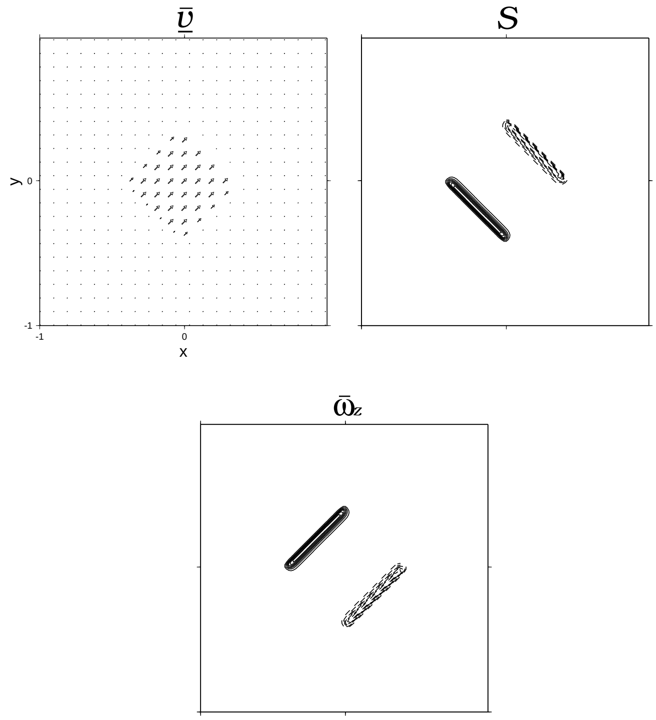

Figure 2. Velocity vectors $\underline{\bar{v}}$, source-sink function (or horizontal divergence) S, and vertical vorticity $\bar{\omega}_z$ for the square plate standard. S and $\bar{\omega}_z$ are described by equations (13) and (14), respectively, with $\alpha = \beta = 0.25$. The maximum nondimensional velocity is 0.045. The maximum and minimum values of both S and $\bar{\omega}_z$ are ± 0.98 and the contour interval is 0.13.

2.4 The Source-Sink Function

In this study we examine only one simple flow pattern to illustrate the basic physics of plate generation. Our source-sink configuration is derived from the motion of a single rectangular plate. A square plate, as shown by Olson & Bercovici (1991) is the simplest paradigm for a tectonic plate. The presumed active tectonic plates (i.e., plates attached to signficant subducting slabs) on the Earth have convergent (subduction) zones that effectively comprise between 20 and 30% of the plates' circumferences (Forsyth & Uyeda 1975); a square plate drifting perpendicular to one of its edges has a convergent zone (i.e., a leading edge) that is precisely 25% of its net circumference. Under such uniform drift, a square plate's kinetic energy is exactly equipartitioned between toroidal and poloidal parts, and an ensemble of independently drifting square plates produces a distribution of plate margins rather closely resembling that of the real Earth. However, most importantly for this study, the toroidal flow field of a rectangular plate is precisely known. Thus we here treat the rectangular plate as the standard we wish to achieve. We separate the poloidal component of the plate's velocity field by taking its horizontal divergence and use it as our source-sink function. The sources and sinks thus represent the trailing and leading edges of the plate, respectively. It remains to our model to generate the strike-slip sides of the plate, i.e., the toroidal motion. We thus use this configuration to determine which rheology best reproduces the original plate.

To derive the source-sink function S, we consider a rectangular plate with sides of length 2α and 2β in the x' and y' directions, respectively; x' and y' are coordinates arbitrarily rotated relative to the x-y axes to allow the plate a general trajectory. The plate moves at a velocity V in the in the y' direction and is surrounded by an immobile medium. At a given instant, we define the origin at the plate's center. The velocity field of the plate as a function of x' and y' is $\bar{v} = VF(x'/\alpha)F(y'/\beta)$. The function F defines the shape of the plate; e.g., for a discontinuous plate F is a step function, i.e.,

$$F(\xi) = \begin{cases} 0 & \xi < -1 \\ 1 & -1 \le \xi \le 1 \\ 0 & \xi > 1 \end{cases} . \tag{11}$$

However, since a discontinuous plate leads to singularities in horizontal divergence and vorticity, we employ an F that is infinitely differentiable. A plate-like shape can be obtained with a slightly modified super-Gaussian, i.e.,

$$F(\xi) = e^{-\xi^{2p}/p}; \quad p \ge 1 \ . \tag{12}$$

For $p = 1$, a regular Gaussian profile is recovered, while in the limits of $p \to \infty$ and $p \to 0$, step- and delta-functions are obtained, respectively. A reasonable step-like plate is obtained for $p > 4$; in this study we exclusively use $p = 8$. With these considerations, we employ a normalized source-sink function:

$$S = \frac{\partial \bar{v}}{\partial y'} = -\left(\frac{2e}{2p-1}\right)^{1-\frac{1}{2p}} \left(\frac{y'}{\beta}\right)^{2p-1} e^{-\frac{1}{p}(x'/\alpha)^{2p}} e^{-\frac{1}{p}(y'/\beta)^{2p}} \tag{13}$$

In this study, the x'-y' axes are rotated clockwise $45°$ relative to the x-y frame; i.e., $(x', y') = (x - y, x + y)/\sqrt{2}$. The rotation of the plate and hence the source-sink field is done to avoid roll-like flows caused by the periodic boundaries employed in the spectral-transform method. Similarly, the plates vertical vorticity is, for later comparison to the dynamically generated vorticity,

$$\bar{\omega_z} = \hat{z}\cdot\nabla\times\underline{\bar{v}} = \frac{\partial\bar{v}}{\partial x'}$$

$$= -\frac{\beta}{\alpha}\left(\frac{2e}{2p-1}\right)^{1-\frac{1}{2p}}\left(\frac{x'}{\alpha}\right)^{2p-1} e^{-\frac{1}{p}(x'/\alpha)^{2p}} e^{-\frac{1}{p}(y'/\beta)^{2p}} \tag{14}$$

For a square plate ($\alpha = \beta$) S and ω_z map precisely into one another by interchanging x' and y'. Thus, because of equation (3), and since $\bar{\omega_z} = -\nabla_h^2\bar{\psi}$ (where $\bar{\psi}$ is the toroidal potential, or stream function, for the plate), the net kinetic energy of a square plate is equipartitioned between poloidal and toroidal parts. That is, since both the toroidal and poloidal potentials satisfy Poisson's equation for forcing functions which differ only by a rotation of axes, then the toroidal and poloidal flow fields also only differ by a coordinate rotation, and thus bear the same kinetic energy (see also Olson & Bercovici 1991). Figure 2 shows the velocity field $\underline{\bar{v}}$, source-sink function S and vertical vorticity $\bar{\omega_z}$ for a square plate with $\alpha = \beta = 0.25$ and $p = 8$.

The success of our continuum model relies on its ability to reproduce

(i) the plates original vorticity $\bar{\omega_z}$
(ii) kinetic energy equipartitioning given the S derived from a square plate
(iii) the original plate's functional dependence of the toroidal to poloidal kinetic energy ratio on β/α
(iv) the strength (or viscosity) distribution of the plate and surrounding flow; a perfect plate has a uniform strength distribution in its interior with distinctly weak margins.

It should be noted that the actual tectonic plates do not satisfy ideal plate behavior since intraplate deformation is certainly significant. However, the precise quality of plate-like behavior at the Earth's surface is difficult (if not impossible) to assess and quantify; this is of course why the plate tectonic model, wherein the plates are assumed ideal or rigid, is used to determine surface velocities. Therefore, for the sake of simplicity we seek to attain the well defined but perhaps most difficult goal of ideal plate behavior.

3 NUMERICAL EXPERIMENTS: RESULTS AND ANALYSIS

The following results are generated by the numerical solution of equation (5) (combined with equation (3)) on a 256×256 grid with the rheology of equation (6) and the source-sink function of equation (13); see Appendix for further details about the numerical solutions. The domain aspect ratio b is held constant at 1 and the parameter p is kept at 8. The rheological parameters γ and ν, and the plate aspect ratio β/α are varied. For the power-law cases, we allow ν to be as high as 21 to display possible asymptotic behavior of various quantities as $\nu \to \infty$. Furthermore, although the deep mantle is probably characterized by $\nu \approx 3$, it is doubtful that such a low power-law index is sufficient to capture the behavior of the entire plate-mantle system (see Christensen & Harder 1991; Weinstein & Olson 1992).

In Figure 3, we show the velocity vector field $\underline{v}$, contours of the generated vorticity $\omega_z = -\nabla_h^2\psi$, and dimensionless viscosity η for non-Newtonian flow driven by the source-sink function of Figure 2; rheologies include selected power-law cases ($\nu \geq 1$) and the W-G stick-slip case ($\nu = -1$). The velocity field for $\nu = 1$,

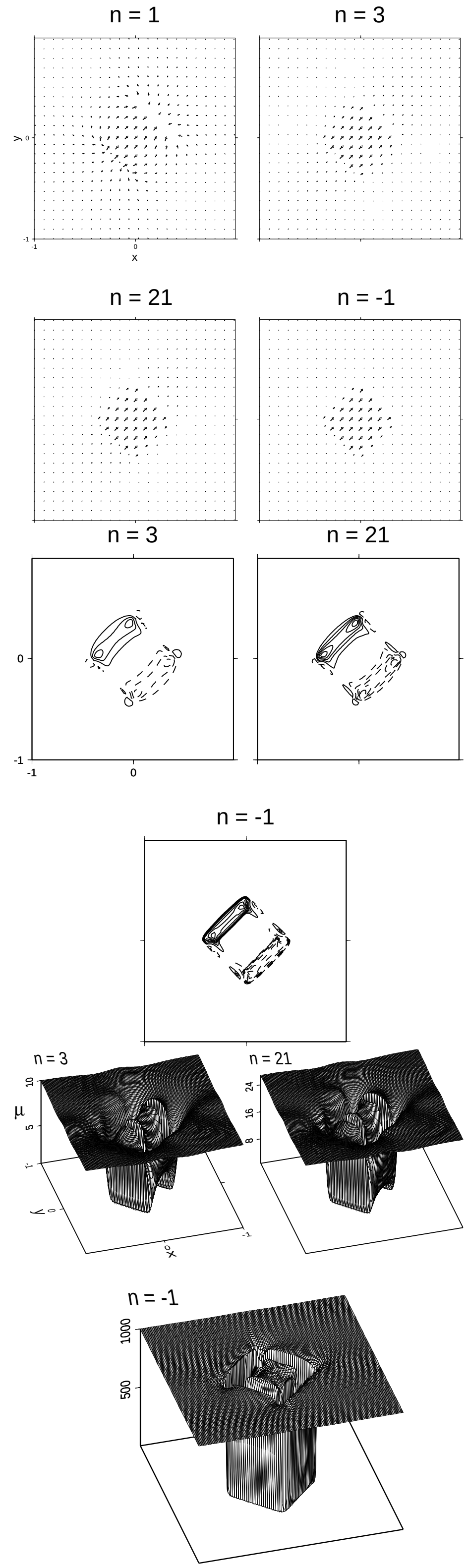

Figure 3. Velocity vectors $\underline{v}$ (a), contours of vertical vorticity ω_z (b), and a three-dimensional surface representation of viscosity η (c), for non-Newtonian flow driven by the source-sink function of Figure 2 with various values of power-law index ν and $\gamma = 10^{-3}$. Vorticity and viscosity for $\nu = 1$ are not shown since, for that case, $\omega_z = 0$ and η is constant. The maximum velocity for $\nu = 1,\ 3,\ 21$ and -1 are 0.026, 0.039, 0.042 and 0.046, respectively. The maximum and minimum vorticity for $\nu = 3,\ 21$ and -1 are, $\pm0.22,\ \pm0.34$ and ±0.46, respectively; the vorticity contour interval is 0.061 for all values of ν.

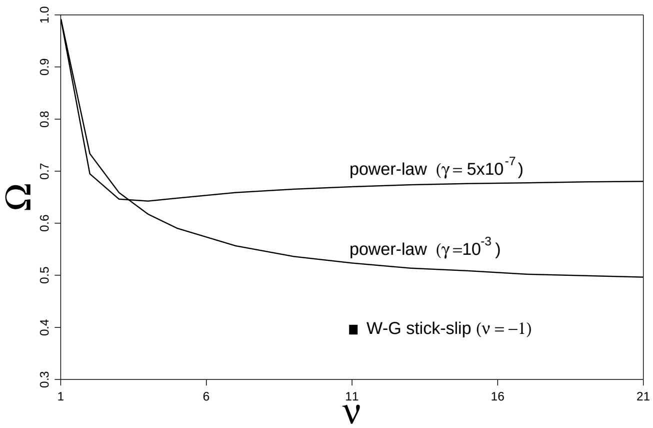

Figure 4. Vorticity deviation Ω, defined in equation (15), versus power-law index ν for the source-sink function of Figure 2 and the power-law rheology ($\nu \geq 1$) and two different values of γ. The value of Ω for the W-G stick-slip rheology (with $\gamma = 10^{-3}$) is shown for comparison.

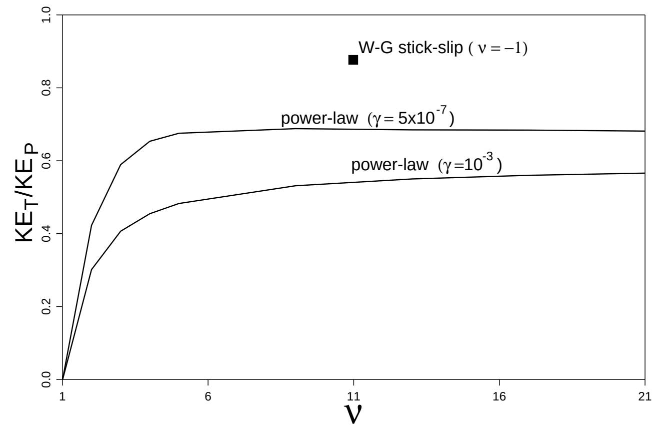

Figure 5. The ratio of toroidal to poloidal kinetic energy KE_T/KE_P versus ν for the same cases as Figure 4.

the Newtonian case, is shown to illustrate completely irrotational flow, i.e., when $\psi = 0$. Clearly, the velocity and vorticity fields become more like those of the original square plate as ν increases to 21; yet, they are most similar to the fields of the square plate, in shape and magnitude, for the W-G stick-slip rheology ($\nu = -1$). However, while the largest generated velocity (for the W-G case) is essentially the same as that for the original plate, the maximum generated vorticity (again for the W-G case) is less than half that of the square plate.

The viscosity field (Figure 3c) changes little in shape in the power-law cases for $\nu \geq 3$. The W-G stick-slip case, however, is quite distinct, producing the most plate-like strength distribution. In all cases, the viscosity lows are aligned with concentrations in S and ω_z; yet the lows are most sharply defined for the W-G rheology. Furthermore, the W-G rheology produces nearly uniform high viscosity regions in the plate interior and the medium surrounding the plate. In the power-law cases, even for very high ν, the viscosity of the plate region is strongly spatially varying, maintaining a distinct saddle-shape.

A quantitative measure of how closely the induced toroidal flow matches that of the original plate is contained in a quantity we call the vorticity deviation

$$\Omega = \frac{\int_A (\omega_z - \bar{\omega_z})^2 dA}{\int_A \bar{\omega_z}^2 dA} \tag{15}$$

where $dA = dxdy$ and A is the area contained in the domain $-1 \leq x, y/b \leq 1$. The vorticity deviation contains information not only about the ratio of amplitudes of the two vorticities (the term in equation (15) that goes as $\int_A \omega_z^2 dA / \int_A \bar{\omega_z}^2 dA$) but also the spatial correlation between the vorticities (the cross term that goes as $\int_A \omega_z \bar{\omega_z} dA / \int_A \bar{\omega_z}^2 dA$). A perfect match between ω_z and $\bar{\omega_z}$ yields $\Omega = 0$. Assuming that the Newtonian case ($\nu = 1$), which can generate no vorticity, produces the worst match, then $\Omega = 1$ represents the poorest fit. While it is conceivable that there are even worse fits than in the Newtonian case (e.g., dilatancy cases, in which $0 < \nu < 1$, produce weak plate interiors and strong margins), for these strain-rate softening rheologies, Ω is never > 1.

Figure 4 shows Ω versus ν for the power-law cases ($1 \leq \nu \leq 21$) and, for comparison, the value of Ω for the W-G stick-slip case ($\nu = -1$); in all cases $\alpha = \beta = 0.25$. The W-G case has $\gamma = 10^{-3}$, yielding a maximum dimensionless viscosity of 1000. Two curves are shown for the power-law cases. One curve has the same γ as the W-G case, and the other has a $\gamma = 5 \times 10^{-7}$ such that the maximum viscosity at $\nu = 21$ is the same as that for the W-G case. This is done to avoid any inequitable comparisons.

The largest vorticity deviation occurs at $\nu = 1$, as expected. For the power-law cases, the minimum deviation is approximately 0.5. While the solutions with largest viscosity contrast (i.e., with $\gamma = 5 \times 10^{-7}$) yield more plate-like characteristic in other categories (e.g., kinetic energy partitioning; see below), they display larger vorticity deviation than for the cases with $\gamma = 10^{-3}$, approaching $\Omega = 0.7$ as $\nu \rightarrow 21$. One of the most interesting features of the power-law cases is that Ω appears to reach an asymptote as $\nu \rightarrow \infty$. This implies that a power-law rheology has an upper limit on how well it can produce a plate-like vorticity. The vorticity deviation for the W-G stick-slip rheology is shown for comparison; at 0.4, it is the lowest value shown in Figure 4.

The toroidal to poloidal kinetic energy ratio

$$KE_T/KE_P = \frac{\int_A |\nabla_h \psi|^2 dA}{\int_A |\nabla_h \phi|^2 dA} \tag{16}$$

versus ν is shown in Figure 5 for the same cases as in Figure 4. For an ideal square plate this ratio is unity, while for a Newtonian fluid it is zero. For the power-law cases with $\gamma = 10^{-3}$ and $\gamma = 5 \times 10^{-7}$, KE_T/KE_P approachs 0.5 and 0.65, respectively, as $\nu \rightarrow 21$. In this category, the higher viscosity contrast cases yield better plate-like behavior. However, as with vorticity deviation, the kinetic energy partitioning appears to reach an asymptotic value as $\nu \rightarrow \infty$, again suggesting that the power-law rheology is limited in its ability to produce plate-like flows. In contrast to the power-law cases, the W-G stick-slip rheology yields the largest KE_T/KE_P shown of 0.88, a quite reasonable reproduction of the ideal plate partitioning.

For completeness, we show in Figure 6 Ω and KE_T/KE_P versus ν for several stick-slip cases with $-10 \leq \nu < 0$ and $\gamma = 10^{-3}$. The minimum vorticity deviation of 0.3 occurs at $\nu = -2$, while the maximum KE_T/KE_P of 0.9 occurs at $\nu = -0.3$. In these categories, the stick-slip rheologies clearly are more successful at reproducing the ideal square plate.

Finally, we examine the dependence of KE_T/KE_P on the aspect ratio β/α (Figure 7). For the ideal rectangular plate, $KE_T/KE_P \approx \beta/\alpha$, as shown by the dashed curve in Figure 7. This differs from the plate model used by Olson & Bercovici (1991) wherein $KE_T/KE_P = (\beta/\alpha)^2$; in that study, the domain size and plate size were linearly dependent, whereas here they are

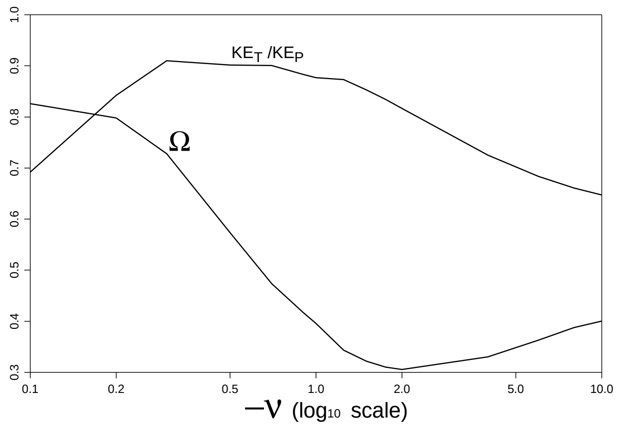

Figure 6. Vorticity deviation Ω and kinetic energy ratio KE_T/KE_P for the stick-slip cases with $\nu < 0$ and the source-sink function of Figure 2. For all cases $\gamma = 10^{-3}$.

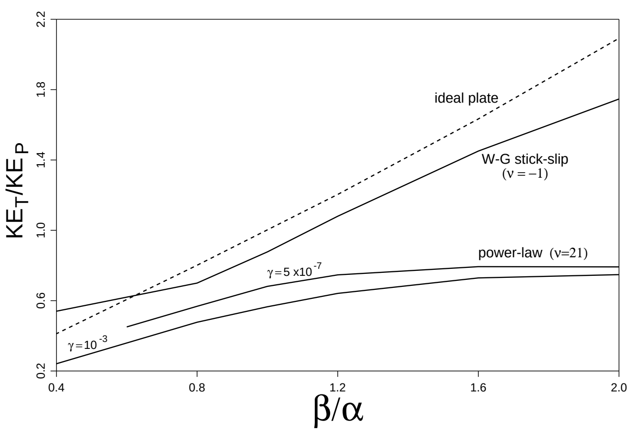

Figure 7. Kinetic energy ratio KE_T/KE_P versus plate aspect ratio β/α for the source-sink function derived from the velocity field of a general rectangular plate. Curves are shown for the power-law rheology with $\nu = 21$ (and two values of γ) and the W-G stick-slip rheology with $\nu = -1$ (and $\gamma = 10^{-3}$). The dashed curve shows KE_T/KE_P for the original, ideal rectangular plate

independent. Figure 7 also shows KE_T/KE_P versus β/α for the power-law rheology with $\nu = 21$ and the W-G stick-slip rheology. The same values of γ as Figures 4 and 5 are used and α is held constant at 0.25. Although, the power-law case does yield an increase in KE_T/KE_P with increasing β/α, its curves diverge considerably from that of the ideal plate and do not even achieve equipartitioning as $\beta/\alpha \to 2$. In contrast, KE_T/KE_P for the W-G rheology follows the curve for the ideal plate relatively closely, and exceeds equipartitioning at $\beta/\alpha = 1.2$.

4 DISCUSSION

4.1 Power-Law versus Stick-Slip Rheologies

The results of this study suggest that plate-like flow, and hence the generation of plate tectonics from mantle convection, is not readily attained with a power-law rheology, not with a mantle-type law with $\nu = 3$, nor an extreme one with $\nu = 21$ (or perhaps, as suggested, even in the limit of $\nu \to \infty$). A power-law rheology has always been employed in the past as it is what experimental evidence has provided. However, although pseudo-plasticity may yield strong plates and weak margins, it is far from a comprehensive model of the various failure mechanisms (especially discontinuous brittle failure) in the Earth's lithosphere. Furthermore, nonisothermal effects (frictional heating) are not accounted for in rheometric experiments. The myriad influences of water, suggested to be a primary cause for the Earth's unique version of tectonics (e.g., see Kaula 1990), may also not be appropriately accounted for in the power-law rheology. Although rheometric experiments have been performed with wet silicates (e.g., Chopra & Paterson 1981, 1984), the influence of water on melting at ridges, serpentinization of peridotite at transforms (Bonatti 1978), lubrication of subduction by muds and enhancement of pore pressure (Shreve & Cloos 1986), has yet to be comprehensively accounted for in a single rheology (see Kirby & Kronenberg 1987 for review). While it is unlikely that a single rheology could in actuality incorporate all these effects, it is important to recognize that the power-law rheology may be wholly inadequate for describing the plate-mantle system.

In this study, the rheology that is most successful at producing plates is the hypothetical stick-slip or self-lubricating rheology with $\nu < 0$. The stick-slip rheology does not represent any empirical or physically rigorous rheology. However, it does capture an important physical effect which may aid in understanding what rheology is necessary to generate plates. The stick-slip rheology is better at producing plate-like flow than the power-law rheology because, as shown earlier, the stress–strain-rate relation is monotonic for the power-law case, but non-monotonic for the stick-slip case (see Figure 1). Thus, in the stick-slip case if the maximum strain-rate in the flow exceeds $\sqrt{-\nu\gamma}$, there can be a local stress minimum at the strain-rate maximum; i.e., in the zones of fastest deformation, there can be a stress minimum (though not necessarily the minimum stress). It is this property which allows the stick-slip rheology to yield the best plate-like behavior. This can be understood by considering the transfer of momentum from the edge of a moving plate (or wall) to a neighboring infinite viscous medium. The plate moves in the positive y-direction with its edge at $x = 0$; the fluid extends to the left to $x = -\infty$. The strain-rate is always largest at the plate edge as the fluid only comes into equilibrium as time $t \to \infty$. In a Newtonian or power-law fluid, the shear stress $\sigma_{xy} = \eta\frac{\partial v}{\partial x}$ is also largest at the wall, as illustrated in Figure 8, and decreases as $x \to -\infty$. The force (per unit volume) on the fluid in the y-direction is $f_y = \frac{\partial \sigma_{xy}}{\partial x}$, which for all power-law cases is always > 0. Thus a positive force is exerted by the plate on all parts of the fluid; this force acts to bring the fluid into equilibrium with the plate. Momentum is always transferred outward from the plate into the fluid.

In the stick-slip case, however, if the strain-rate maximum at the plate's edge is $> \sqrt{-\nu\gamma}$, then a stress minimum is at the plate's edge; the stress maximum occurs at some $x \neq 0$ where the strain-rate is $\sqrt{-\nu\gamma}$. Physically, this implies that the fluid is so weakened near the wall that the strong (high viscosity) fluid actually retains more stress than fluid at the wall. Since stress decreases toward the plate's edge, the region of fluid between the stress maximum and the plate edge has a retrograde force on it, i.e., $f_y < 0$. This reverse force causes the weak fluid by the wall to decelerate, thus inducing the velocity profile near the wall to sharpen. The sharpening of the velocity profile causes the shear strain-rate to increase, the shear stress near the wall thereby to decrease, and thus the retrograde force to increase further. The cycle continues, constituting a feedback mechanism which causes the velocity profile in the fluid to become plate-like.

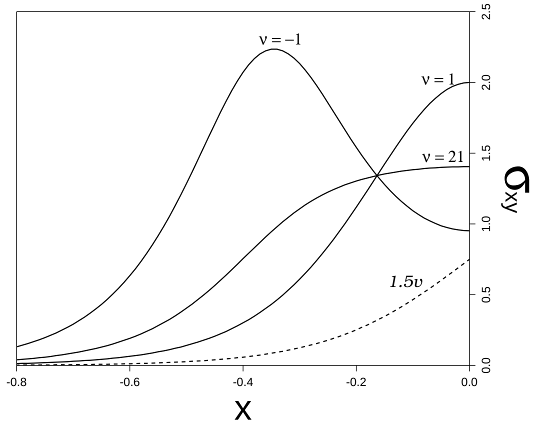

Figure 8. An illustration of shear stress σ_{xy} imparted to a fluid half-space (extending to $x = -\infty$) by a plate (or wall) at $x = 0$ moving in the $+y$-direction. Stress is determined for several non-Newtonian rheologies for an arbitrary velocity prescribed to be $v = \frac{1}{2}[1 + \tanh(4x)]$ at a given instant in time; velocity (increased by 50%) is shown by the dashed curve.

4.2 Boundary Layer Theory

The above arguments can be demonstrated more rigorously with a simple boundary layer theory. The above idealization is described by the dimensional momentum equation, in this case

$$\frac{\partial v}{\partial t} = \frac{1}{\rho}\frac{\partial}{\partial x}\left(\eta\frac{\partial v}{\partial x}\right) \tag{17}$$

where the acceleration term is retained because the fluid domain is an infinite half-space and cannot, therefore, ever be in equilibrium. To be able to employ similarity arguments, we take the limit of $\gamma = 0$; in this case, the stress maximum for flow with the stick-slip rheology occurs at $x = -\infty$. Viscosity is thus defined as

$$\eta = A\left(\frac{\partial v}{\partial x}\right)^{1/\nu - 1}. \tag{18}$$

where A is a constant. We assume that v is only dependent on the similarity variable $\zeta = x/\delta(t)$, where $\delta(t)$ is the thickness of the velocity boundary layer. Combining equations (17) and (18), using $v = v(\zeta)$, and, after some manipulation, integrating the resulting equation over the extent of the boundary layer, i.e., over $-1 \le \zeta \le 0$, leads to an equation for δ:

$$\delta^{1/\nu}\frac{d\delta}{dt} = -\frac{A[v'(0) - v'(-1)]}{\rho\nu\int_{-1}^{0}\zeta\left(dv/d\zeta\right)^{2-1/\nu}d\zeta} \tag{19}$$

The growth of the boundary layer, determined by equation (19), represents the transfer of momentum from the plate edge to the adjacent medium (since the size of δ is indicative of the amount of fluid dragged along by the plate). At the plate edge $v = V$, and at the extent of the boundary layer (i.e., at $\zeta = -1$) $v \approx 0$. We thus approximate the velocity within the boundary layer as $v = V(\zeta + 1)^3$. The cubic function is chosen so that v, its slope and curvature are continuous with the essentially unmoving fluid beyond the boundary layer; i.e., $v = v' = v'' = 0$ at $\zeta = -1$. In this case, integration of equation (19) yields

$$\delta = \begin{cases} \left[\frac{A(6\nu-2)(5\nu-2)(\nu+1)}{\rho\nu^4(3V)^{1-1/\nu}}t + C\right]^{\frac{\nu}{\nu+1}} & \nu \neq -1 \\ \delta_o e^{-\frac{56A}{\rho(3V)^2}t} & \nu = -1 \end{cases} \tag{20}$$

where C and δ_o are arbitrary integration constants (see also Bird, Stewart & Lightfoot 1960, ch. 4). (Equation (20) is not valid when $\nu = \frac{1}{3}$ or $\nu = \frac{2}{5}$; however, since we are mainly interested in rheologies with $\nu \ge 1$ and $\nu < 0$, we will not concern ourselves with these special cases.) For the power-law cases with $\nu > 1$, the constant $C = 0$ if the plate's motion begins instantaneously (i.e., $\delta = 0$ at $t = 0$). Thus, the velocity boundary layer thickness always grows for $\nu > 1$. Momentum is always transferred away from the plate, even for very large ν. However, in the stick-slip cases with $\nu < 0$, δ can diminish with time, depending on the choice of C; in the W-G case of $\nu = -1$, δ can only shrink with time. Thus, the velocity profile can sharpen (and must sharpen for $\nu = -1$) near the plate edge. Momentum transfer can thus be inhibitted or blocked altogether for the stick-slip rheologies.

The stick-slip rheologies, therefore, can cause velocity profiles to sharpen into plate-like flows and can reduce or eliminate the transfer of momentum from a fast moving region to a slower one. This property allows for the generation of a distinct plate-like flow that is decoupled from the surrounding medium; i.e., outlying resistive forces that act to smooth the flow and distribute momentum are greatly reduced. In short, this rheology provides for the forming of the plates as well as efficient lubrication of its edges.

5 CONCLUSIONS

We have employed a relatively simple model of source-sink driven, non-Newtonian lithospheric flow to determine what rheology allows for the most efficient generation of tectonic plates. We chose as our standard a rectangular plate drifting perpendicular to one of its edges. The horizontal divergence of the plate's velocity was used as a source-sink function (where a source occurs at the trailing edge, and a sink occurs at the leading edge). This function was then applied to the model to drive fluid flow for various non-Newtonian rheologies to determine which rheologies best reproduced the original rectangular plate. The rheologies used included a range of power-law (i.e., pseudo-plastic Carreau) relations and a theoretical rheology that models stick-slip behavior.

In the limit of Newtonian flow, no plate-like behavior is generated, as expected. As the power-law index ν is increased, the power-law rheology appears to reach an asymptotic limit in its rather modest ability to generate plate-like behavior. The stick-slip rheologies, while not able to generate the ideal plate, are considerably more successful at producing plate-like flows. An analysis of momentum transfer and a boundary-layer theory indicates that the stick-slip rheology is more successful at generating plates because it can cause velocity profiles to sharpen and impedes or prohibits the transfer of momentum from the plate-like flow to the surrounding medium; i.e., it induces considerable lubrication.

These results imply that the non-Newtonian rheology that can best describe plate behavior is one that not only permits strain-rate softening (and thus strong plate interiors and weak plate margins) but also a negative feedback between stress and strain-rate. The latter effect (the negative feedback) leads to sharpening of plate edges as well as lubrication of plate margins (see also Schubert & Turcotte 1972). The negative feedback mechanism may also be facilitated by the presence of water (as lubrication certainly is), and this is in line with present theories of the role of water at plate margins and why Earth appears to be the only planet with clearly defined plate tectonics. Although the stick-slip rheologies used in this study are merely hypothetical, they indicate that the rheologies required to allow plate tectonics to arise from mantle convection must incorporate mechanisms not accounted for by standard mantle rheologies.

ACKNOWLEDGMENTS

The author is grateful for helpful discussions with Peter Olson and Pål Wessel, and for thoughtful comments from two anonymous reviewers. This work was supported by NASA through grant NAGW-3015.

References

Beaumont, C., 1976. The evolution of sedimentary basins on a viscoelastic lithosphere, *Geophys. J. R. Astron. Soc.*, **55**, 471–497.

Bercovici, D., Schubert, G., & Glatzmaier G. A., 1989. Three-dimensional, spherical models of convection in the Earth's mantle, *Science*, **244**, 950–955.

Bird, R. B., Stewart, W. E. & Lightfoot, E. N., 1960. *Transport Phenomena*, John Wiley, New York.

Bird, R. B., Armstrong, R. C. & Hassager, O., 1987. *Dynamics of Polymeric Liquids* vol. 1, Wiley Interscience, New York.

Bonatti, E., 1978. Vertical tectonism in oceanic fracture zones, *Earth Planet. Sci. Lett.*, **37**, 369–379.

Chopra, P. N., & Paterson, M. S., 1981. The experimental deformation of dunites, *Tectonophysics*, **78**, 453–473.

Chopra, P. N., & Paterson, M. S., 1984. The role of water in the deformation of dunite, *J. Geophys. Res.*, **89**, 7861–7876.

Christensen, U., 1984. Convection with pressure- and temperature-dependent non-Newtonian rheology, *Geophys. J. R. astron. Soc.*, **77**, 343–384.

Christensen, U. & Harder, H., 1991. Three-dimensional convection with variable viscosity, *Geophys. J. Int.*, **104**, 213-226.

Cserepes, L., 1982. Numerical studies of non-Newtonian mantle convection, *Phys. Earth Planet. Int.* **30**, 49-61.

Cserepes, L. & Christensen, U. 1990. Three-dimensional convection under drifting plates, *Geophys. Res. Lett.* **17**, 1497-1500.

Davies, G.F., 1986. Mantle convection under simulated plates: effects of heating modes and ridge and trench migration, and implications for the core-mantle boundary, bathymetry, the geoid and Benioff zones, *Geophys. J. Roy. Astron. Soc.* **84**, 153-183.

Davies, G.F., 1989. Mantle convection model with a dynamic plate: topography, heat flow and gravity anomalies, *Geophys. J.* **98**, 461-464, 1989.

Forsyth, D. & Uyeda, S., 1975. On the relative importance of the driving forces of plate motion, *Geophys. J. R. astr. Soc.*, **43**, 163–200.

Forte, A.M. & Peltier, W. R., 1987. Plate tectonics and aspherical earth structure: the importance of poloidal-toroidal coupling, *J. Geophys. Res.*, **92**, 3546-3680.

Forte, A.M., Peltier, W. R. & Dziewonski, A. M., 1991. Inferences of mantle viscosity from tectonic plate velocities, *Geophys. Res. Lett.*, **18**, 1747–1750.

Gable, C. W., O'Connell, R. J. & Travis, B. J., 1991., Convection in three dimensions with surface plates: Generation of toroidal flow, *J. Geophys. Res.*, **96** , 8391–8405.

Gurnis, M., 1988. Large-scale mantle convection and the aggregation and dispersal of supercontinents, *Nature*, **332**, 695-699.

Gurnis, M. & Hager, B. H., 1988. Controls of the structure of subducted slabs, *Nature*, **335**, 317–321.

Hager, B. H. & O'Connell, R. J., 1978. Subduction zone dip angles and flow driven by plate motion, *Tectonophysics*, **50**, 111–133.

Hager, B. H. & O'Connell, R. J., 1979. Kinematic models of large-scale flow in the Earth's mantle, *J. Geophys. Res.*, **84**, 1031–1048.

Hager, B.H. & O'Connell, R. J., 1981. A simple global model of plate dynamics and mantle convection, *J. Geophys. Res.*, **86**, 4843–4867.

Holmes, A., 1928. Radioactivity and Earth movements, *Trans. Geol. Soc. Glasgow*, **18**, 559–606.

Houseman, G., 1988. The dependence of convection planform on mode of heating, *Nature*, **332**, 346–349.

Kaula, W. M., 1980. Material properties for mantle convection consistent with observed surface fields, *J. Geopys. Res.*, **85**, 7031-7044, 1980.

Kaula, W. M., 1990. Venus: a contrast in evolution to Earth, *Science*, **247**, 1191–1196.

King, S. D. & Hager, B. H., 1990, The relationship between plate velocity and trench viscosity in Newtonian and power-law subduction calculations, *Geophys. Res. Lett.*, **17**, 2409–2412.

King, S. D., Gable, C. W. & Weinstein, S. A., 1992. Models of convection-driven plates: a comparison of methods and results, *Geophys. J. R. astr. Soc.*, **109**, 481–487.

Kirby, S. H. & Kronenberg, A. K., 1987. Rheology of the lithosphere: selected topics, *Rev. Geophys.*, **25**, 1219–1244.

Lachenbruch, A. H., 1976. Dynamics of a passive spreading center, *J. Geophys. Res.*, **81**, 1883-1902.

O'Connell, R. J., Gable, C. W. & Hager, B. H., 1991. Toroidal-poloidal partitioning of lithospheric plate motion, in *Glacial Isostasy, Sea Level and Mantle Rheology*, pp 535–551, eds Sabadini, R. et al., Kluwer Academic Publishers, Dordrecht.

Olson, P. & Bercovici, D., 1991. On the equipartitioning of kinetic energy in plate tectonics, *Geophys. Res. Lett.*, **18**, 1751-1754.

Olson, P. & Corcos, G. M., 1980. A boundary layer model for mantle convection with surface plates, *Geophys. J. R. astr. Soc.*, **62**, 195–219.

Olson, P. & Hagee, V. L., 1990. Geomagnetic polarity reversals, transition field structure, and convection in the outer core, *J. Geophys. Res.*, **95**, 4609–4620.

Orszag, S. A., 1971. Numerical simulation of incompressible flows within simple boundaries. I. Galerkin (spectral) representations, *Stud. Appl. Math.*, **4**, 293–327.

Orszag, S. A., 1980. Spectral methods for problems in complex geometries, *J. Comp. Phys.*, **37**, 70–92.

Parmentier, E. M., 1978. A study of thermal convection in non-Newtonian fluids, *J. Fluid Mech.*, **84**, 1–11.

Parmentier, E. M., Turcotte, D. L., & Torrance, K. E., 1976. Studies of finite amplitude non-Newtonian thermal convection with applications to convection in the Earth's mantle, *J. Geophys. Res.* **81**, 1839–1846.

Parmentier, E. M. & Morgan, J., 1982. Thermal convection in non-Newtonian fluids: Volumetric heating and boundary layer scaling, *J. Geophys. Res.*, **87**, 7757–7762.

Ranalli, G., 1987. *Rheology of the Earth*, Allen & Unwin Publishers, Winchester, Mass.

Ribe, N. M., 1992. The dynamics of thin shells with variable viscosity and the origin of toroidal flow in the mantle, *Geophys. J. Int.*, **110**, 537–552.

Ricard, Y. & Bai, W., 1991. Inferring the viscosity and the 3-D density structure of the mantle from geoid, topography and plate velocities, *Geophys. J. Int.*, **105**, 561–571.

Ricard, Y., & Vigny C., 1989. Mantle dynamics with induced plate tectonics, *J. Geophys. Res.*, **94**, 17543-17559.

Ricard, Y., Froidevaux, C. & Fleitout, L., 1988. Global plate motion and the geoid: a physical model, *Geophys. J.*, **93**, 477-484.

Roberts, P. H. & Soward, A. M., 1992. Dynamo theory, *Ann. Rev. Fluid Mech.*, **24**, 459–512.

Schubert, G. & Turcotte, D. L., 1972. One-dimensional model of shallow mantle convection, *J. Geophys. Res.*, **77**, 945–951.

Shreve, R. L. & Cloos, M., 1986. Dynamics of sediment subduction, malange formation, and prism accretion, *J. Geophys. Res.*, **91**, 10229–10245.

Turcotte, D. L. & Oxburgh, E. R., 1967. Finite amplitude convective cells and continental drift, *J. Fluid Mech.*, **28**, 29–42.

Watts, A. B., Karner G. D. & Steckler, M. S., 1982. Lithospheric flexure and the evolution of sedimentary basins, *Philos. Trans. R. Soc. London, Ser. A*, **305**, 249–281.

Weertman, J. & Weertman, J. R., 1975. High temperature creep of rock and mantle viscosity, *Ann. Rev. Earth Planet. Sci.*, **3**, 293–315.

Weinstein, S. & Olson, P., 1992. Thermal convection with non-Newtonian plates, *Geophys. J. Int.*, **111** 515–530.

Whitehead, J. A. & Gans, R. F., 1974. A new, theoretically tractable earthquake model, *Geophys. J. R. astr. Soc.*, **39**, 11–28.

Yuen, D. A. & Schubert, G., 1979. The role of shear heating in the dynamics of large ice masses, *J. Glaciol.*, **24**, 195–212.

Appendix: Solution Method

The dimensionless toroidal and poloidal functions ψ and ϕ are assumed periodic over the domain with period 2 in the x-direction and $2b$ in the y-direction. Thus

$$(\psi, \phi) = \sum_{m=-\infty}^{\infty} \sum_{n=-\infty}^{\infty} (\Psi_{mn}, \Phi_{mn}) e^{im\pi x} e^{in\pi y/b} \ . \qquad (A1)$$

The infinite series are truncated at $m, n = \pm N/2$. From equation (3), Φ_{mn} is automatically prescribed by

$$\Phi_{mn} = -S_{mn}/k_{mn}^2 \qquad (A2)$$

where $k_{mn}^2 = \pi^2(m^2 + n^2/b^2)$ and

$$S_{mn} = \frac{1}{4b} \int_{-1}^{+1} \int_{-b}^{+b} S(x,y) e^{-im\pi x} e^{-in\pi y/b} dx dy \ . \qquad (A3)$$

In most cases, our rheological law involves an irrational function of derivatives of ψ and ϕ, thus there is no guarantee that our viscosity field has the same periodicity as assumed for ψ and ϕ. Any apparent linear trend in viscosity across one fundamental period of the domain will lead to spurious high wavenumber noise in a Fourier representation of η; this occurs because linear trends lead to discontinuities at the boundaries of the domain. To treat linear trends in η separately from the Fourier representation, we assume, regardless of rheology, that

$$\eta = a_o + a_1 x + a_2 y + a_3 xy + \eta'(x,y) \ . \qquad (A4)$$

The polynomial portion defines a two-dimensional function that approximates the linear trend in η; the four a_i are determined, for speed and simplicity, by requiring this function to coincide with η at the four corners of the domain, i.e., at $x = \pm 1, y = \pm b$. The remaining viscosity perturbation η' has little, if any, spurious high wave-number modes from edge discontinuites. Thus, we may more safely Fourier analyze η'. Equation (5) becomes

$$a_o \nabla_h^4 \psi + \left(2a_1 \frac{\partial}{\partial x} + 2a_2 \frac{\partial}{\partial y} \right) \nabla_h^2 \psi + 4a_3 \frac{\partial^2 \psi}{\partial x \partial y} = B(x,y) \qquad (A5)$$

where $B(x,y)$ contains all the remaining nonlinear and nonconstant-coefficient terms of equation (5). Employing the Fourier representation, equation (A1), we obtain

$$\Psi_{mn} = B_{mn} \Big/ \left[a_o k_{mn}^4 - 2i\pi k_{mn}^2 (m a_1 + n a_2/b) - 4 a_3 m n \pi^2/b \right] \qquad (A6)$$

where

$$B_{mn} = \frac{1}{4b} \int_{-1}^{+1} \int_{-b}^{+b} B(x,y) e^{-im\pi x} e^{-in\pi y/b} dx dy \ . \qquad (A7)$$

Equation (A6) is used to find the Ψ_{mn} for one iteration. Then ψ, ϕ and appropriate derivatives are determined from Ψ_{mn} and Φ_{mn} via use of fast Fourier transforms (FFT), as advocated by Orszag (1971, 1980); clearly, however, ϕ and its derivatives need be calculated only once. From these functions the non-Newtonian viscosity η is calculated from the rheological equation (6). The parameters a_i, $i = 0, 1, 2, 3$, are updated; η' is redetermined and appropriate derivatives of η' are found via FFT's. All nonlinear terms are then consolidated to update $B(x,y)$, which is then transformed via FFT's to B_{mn} and used to solve equation (A6) for Ψ_{mn} on

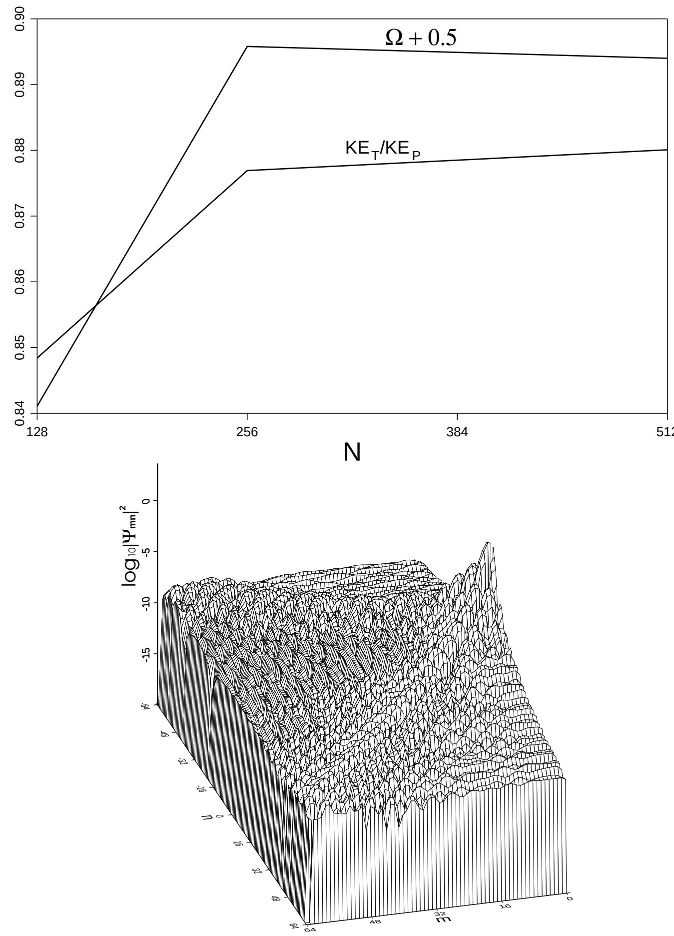

Figure 9. Frame a (top): Vorticity deviation Ω and kinetic energy ratio KE_T/KE_P versus N (the mode at which the Fourier series in the spectral-transform method are truncated; see equation (A1)) for the W-G stick-slip case of Figure 3. Convergence is adequately attained at $N = 256$. Frame b (bottom): Power spectrum of the Fourier coefficients of the toroidal stream function for the W-G stick-slip case of Figure 3 with $N = 256$. Because of dealiasing, power for $|n|, |m| > 64$ is zero and therefore not shown. Since the stream function ψ is a real quantity, coefficients for $\pm m$ are linearly dependent and are therefore combined in the power spectrum. The power undergoes a ten-order of magnitude drop which indicates that the solutions are well resolved.

the next iteration. Aliasing is reduced by setting $B_{mn} = 0$ for $|m|, |n| > N/4$. Under-relaxation is used to facilitate numerical stability. If $\tilde{\Psi_{mn}}$ is the solution to equation (A6) at iteration j, then

$$\Psi_{mn}^{(j)} = \mu\tilde{\Psi_{mn}} + (1-\mu)\Psi_{mn}^{(j-1)} \qquad (A8)$$

where the superscript denotes iteration number; $\mu = 0.9$ yields reasonable and consistent convergence. Iterations proceed until the convergence criterion

$$\frac{\sum_m \sum_n |\Psi_{mn}^{(j)} - \Psi_{mn}^{(j-1)}|^2}{\sum_m \sum_n |\Psi_{mn}^{(j)}|^2} < 10^{-6} \qquad (A9)$$

is satisfied. Solution convergence for increasing N is also tested. The kinetic energy ratio KE_T/KE_P and vorticity deviation Ω vs N (up to $N = 512$) are shown in Figure 9a for one of the most numerically demanding solutions, i.e., the W-G stick-slip case. Convergence is sufficiently attained at $N = 256$ which is employed throughout the paper. Accuracy of solutions is also estimated by examining the power spectrum for Ψ_{mn}. Figure 9b shows the power spectrum also for the W-G case; clearly, a drop of ten orders of magnitude in spectral power implies that the solutions are well resolved.